HHS Public Access

Author manuscript

Cell Rep. Author manuscript; available in PMC 2022 August 24.

Published in final edited form as:

Cell Rep. 2022 June 28; 39(13): 111003. doi:10.1016/j.celrep.2022.111003.

Divergent outer retinal circuits drive image and non-image visual behaviors

Corinne Beier[1,5], **Ulisse Bocchero**[2,5], **Lior Levy**[2], **Zhijing Zhang**[3], **Nange Jin**[3], **Stephen C. Massey**[3], **Christophe P. Ribelayga**[3], **Kirill Martemyanov**[4], **Samer Hattar**[1,*], **Johan Pahlberg**[2,6,*]

[1]Section on Light and Circadian Rhythms, NIMH, NIH, Bethesda, MD 20892, USA

[2]Photoreceptor Physiology Group, NEI, NIH, Bethesda, MD 20892, USA

[3]Ruiz Department of Ophthalmology and Visual Science, UTHealth McGovern Medical School, Houston, TX 77030, USA

[4]Department of Neuroscience, The Scripps Research Institute, Jupiter, FL 33458, USA

[5]These authors contributed equally

[6]Lead contact

SUMMARY

Image- and non-image-forming vision are essential for animal behavior. Here we use genetically modified mouse lines to examine retinal circuits driving image- and non-image-functions. We describe the outer retinal circuits underlying the pupillary light response (PLR) and circadian photoentrainment, two non-image-forming behaviors. Rods and cones signal light increments and decrements through the ON and OFF pathways, respectively. We find that the OFF pathway drives image-forming vision but cannot drive circadian photoentrainment or the PLR. Cone light responses drive image formation but fail to drive the PLR. At photopic levels, rods use the primary and secondary rod pathways to drive the PLR, whereas at the scotopic and mesopic levels, rods use the primary pathway to drive the PLR, and the secondary pathway is insufficient. Circuit dynamics allow rod ON pathways to drive two non-image-forming behaviors across a wide range of light intensities, whereas the OFF pathway is potentially restricted to image formation.

Graphical abstract

*Correspondence: samer.hattar@nih.gov (S.H.), johan.pahlberg@nih.gov (J.P.).

AUTHOR CONTRIBUTIONS

C.B., U.B., K.M., S.H., and J.P. conceptualized the project and designed the methodology. C.B. performed the investigation and data analysis of PLR and circadian photoentrainment experiments. U.B. performed the electrophysiology experiments. U.B. and J.P. analyzed the electrophysiology data. L.L. performed the investigation and data analysis of visual behavior experiments. Z.Z., N.J., S.C.M., and C.P.R. performed the investigation and data analysis of the Cone-Cx36 KO experiments. K.M. provided resources for the experiments. C.B. contributed to writing – original draft preparation. C.B., U.B., L.L., K.M., S.H., and J.P. contributed to writing – review and editing.

SUPPLEMENTAL INFORMATION

Supplemental information can be found online at https://doi.org/10.1016/j.celrep.2022.111003.

DECLARATION OF INTERESTS

The authors declare no competing interests.

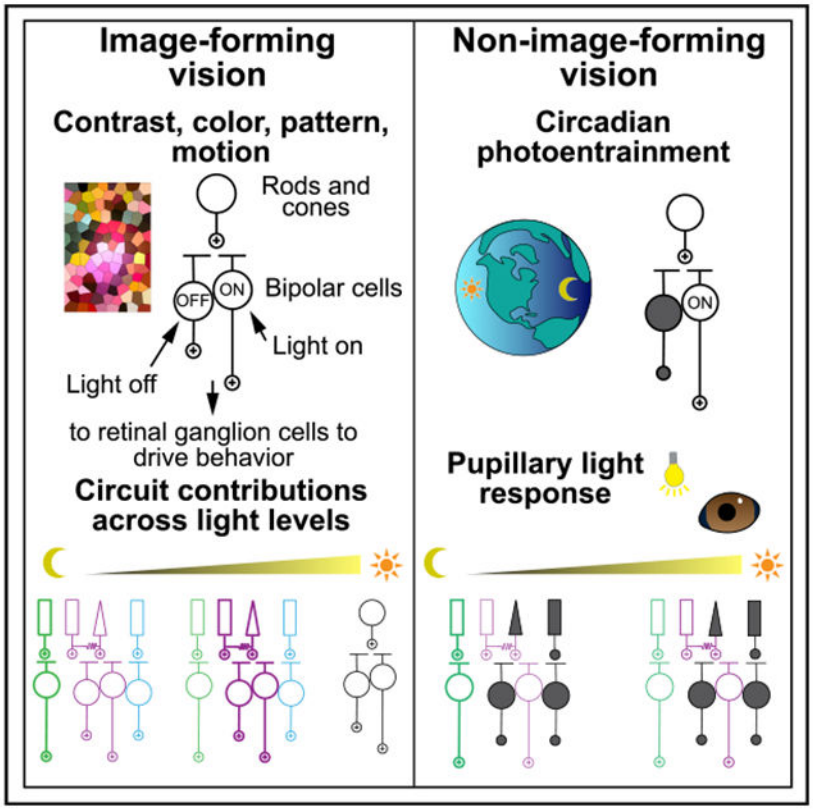

In brief

Beier et al. show that light information diverges at the visual system's first synapse to control major visual functions: image formation and non-image behaviors, such as circadian photoentrainment and pupil constriction. Like image formation, the non-image system depends on the most sensitive retinal circuit under dim light conditions.

INTRODUCTION

Animals perceive their visual environment, consciously and subconsciously, when the retina conveys light information to image-forming and non-image-forming brain regions. In the mammalian retina, there are three types of photoreceptors, the outer retinal photoreceptors, rods and cones, and intrinsically photosensitive retinal ganglion cells (ipRGCs). It has been demonstrated that outer retinal photoreceptors and ipRGCs contribute to non-image-forming behaviors, such as the pupillary light response (PLR) and circadian photoentrainment (Allen et al., 2011; Altimus et al., 2010; Butler and Silver, 2011; Dkhissi-Benyahya et al., 2007; Hattar et al., 2003; Kostic et al., 2016; Lall et al., 2010; Lucas et al., 2001, 2003; Mrosovsky and Hattar, 2003; Panda et al., 2002, 2003; van Oosterhout et al., 2012). The contribution of melanopsin, the photopigment behind the intrinsic light response in ipRGCs, to pupil constriction is limited to high light intensity (Keenan et al., 2016; Lucas et al., 2003). Similarly, melanopsin alone is sufficient to photoentrain animals to bright photoperiods but insufficient in dim photoperiods (Altimus et al., 2010). The rod versus

cone contribution to pupil constriction and circadian photoentrainment is still controversial, but more recent research suggests that rods are the predominant driver of the PLR and circadian photoentrainment (Altimus et al., 2010; Keenan et al., 2016). Surprisingly, even elemental aspects of the outer retinal circuits conveying rod and cone signals to drive non-image-forming behaviors are still unexplored.

For image-forming vision, there are two well-documented parallel pathways, ON and OFF, which respond to the onset and offset of light, respectively (Demb and Singer, 2015; Masland, 2012). This split in information begins at the first synapse in the retina, where cone photoreceptors connect with ON and OFF cone bipolar cells (CBCs). In darkness, photoreceptors release glutamate from their synaptic terminals onto bipolar cell dendrites. ON CBCs are hyperpolarized in response to this release through a transduction pathway that involves metabotropic glutamate receptor 6 (mGluR6) (Masu et al., 1995; Nakajima et al., 1993; Nomura et al., 1994). OFF CBCs, which express ion-otropic glutamate receptors, depolarize in response to glutamate release from photoreceptors. In addition to the ON and OFF cone pathways, there are three rod pathways that are known to contribute to image-forming vision: primary, secondary, and tertiary (Figure 1A; Demb and Singer, 2012; Grimes et al., 2018a; Völgyi et al., 2004). In the primary rod pathway, the most sensitive pathway (Dacheux and Raviola, 1986; Grimes et al., 2018b; Ke et al., 2014), rods synapse with rod bipolar cells (RBCs), which are ON-type cells that also express mGluR6 (Figure 1A, green; Dacheux and Raviola, 1986). In the secondary pathway, rod signals are routed to cones via rod-cone gap junctions and then conveyed to ON and OFF CBCs (Figure 1A, purple; Asteriti et al., 2014; Dacheux and Raviola, 1982; DeVries and Baylor, 1995; Jin et al., 2020; Nelson, 1977). In the tertiary pathway, rods are thought to synapse directly with OFF CBCs (Figure 1A, cyan; Li et al., 2004). Although these pathways have been examined in the context of image-forming vision, it remains unknown whether and how non-image-forming visual behaviors rely on these same pathways.

In this study, we used a multitude of genetically modified mice to systematically dissect the rod and cone pathways in the retina to compare their contributions to non-image-forming behaviors and image-forming vision. We show, using single-cell electrophysiological recordings, that the genetic mutant mouse lines we used silence specific rod and cone circuits. This provides us with the ability to investigate the contribution of distinct rod and cone circuits to the PLR, circadian photoentrainment, and an image-forming visually guided behavioral task. We find that the ON pathway is required for photoreceptor-mediated circadian photoentrainment and normal PLR, whereas the OFF pathway cannot drive these behaviors. In contrast, we show that the OFF pathway is sufficient to drive image-forming vision. This study comprehensively describes the outer retinal circuits driving the PLR across scotopic, mesopic, and photopic light intensities. We show that a non-image-forming visual behavior, the PLR, requires the most sensitive retinal pathway, the primary rod pathway, for normal function. This study reveals similarities and differences in outer retinal circuit contributions to image- and non-image-forming vision.

RESULTS

The OFF pathway cannot drive the PLR

To investigate the outer retinal pathway contributions to non-image-forming vision, we used the PLR because this behavior is quantitative and shows dynamic responses across time. At the first synapse in the retina, light information from rods and cones is sent to ON and OFF bipolar cells (BCs). Rods and cones reduce their glutamate release in response to light onset, which causes ON and OFF BCs to depolarize and hyperpolarize, respectively (Ashmore and Copenhagen, 1980; Euler and Masland, 2000). To isolate the OFF pathway, we silenced the ON pathway using mGluR6 knockout (KO) animals (Maddox et al., 2008). In these animals, the RBCs and ON CBCs should be unresponsive to light, whereas the OFF pathways remain functional (Figure 1B).

We performed whole-cell patch-clamp recordings from dark-adapted retinal slices to demonstrate retinal pathway silencing. For all mutant mouse lines we use in this study, we recorded from the outer retinal cells to show that the non-silenced pathways remain grossly functional. However, it is known that genetically silencing circuit pathways can result in off-target changes that affect parallel circuits and/or will change crosstalk circuit dynamics, and we have not attempted to characterize those changes here because they should not contribute to our conclusions.

Rods in mGluR6 KO and their littermate control mice showed robust light-evoked responses (Figures 1F and 1G; Table 1; Pahlberg et al., 2017). After confirming that rods were functional, we recorded light responses from the immediate downstream neurons, the BCs (Figure 1A). In littermate control mice, RBCs and ON CBCs show robust depolarizing light responses, as expected (Figures 1K–1P; Cao et al., 2012; Field and Rieke, 2002; Okawa et al., 2010). In mGluR6 KO mice, the light response in RBCs and ON CBCs was absent (Figures 1L and 1Q; Xu et al., 2012). In control and mGluR6 KO mice, OFF CBCs had robust hyperpolarizing responses with similar sensitivity (Figures 1U and 1V; Table 1; half maximal flash strength ($I_{1/2}$) was comparable across all genotypes, ANOVA post hoc Tukey's method, $p > 0.52$). These results confirm that the ON pathway is silenced in our mutant mice, whereas the OFF pathway remains functional (Figures 1B–1V).

We used mGluR6 KO mice to study the dark-adapted transient PLR to overhead light (STAR Methods). At photopic levels (100 lux, 73,000 R*/rod/s), mGluR6 KO mice showed impaired pupil constriction (Figures 2A and 2B). These animals exhibited a delayed response (Figures 2A–2C) with a deficit in constriction immediately after light onset compared with controls (Figure 2C; ANOVA post hoc Dunnett's test, $p = 0.002$). We quantified this by measuring the time to half-minimum pupil constriction and found that mGluR6 KO mice were delayed compared with controls (controls 1.5 ± 0.2 s and mGluR6 KO 4.9 ± 1.2 s to half constriction; ANOVA post hoc Dunnett's test, $p = 0.004$). The delay we observed in the PLR resembles the response seen in animals where ipRGCs are the only functioning photoreceptor (Keenan et al., 2016; Lucas et al., 2001). To determine whether the remaining response in mGluR6 KO animals is entirely due to melanopsin (Opn4) phototransduction in ipRGCs and to isolate any remaining photoreceptor-mediated PLR, we tested mGluR6; Opn4 double KO (dKO) animals. The PLR is abolished in mGluR6; Opn4

dKO mice (Figures 2A and 2B). The PLR in Opn4 KO is not significantly different from littermate controls (Keenan et al., 2016; Lucas et al., 2003; data not shown). Therefore, at photopic light levels, the ON pathway and melanopsin together drive the PLR. The OFF pathway cannot drive the photopic PLR.

The OFF pathway cannot drive circadian photoentrainment

The OFF pathway cannot drive the PLR, but this behavior is predicated on detecting light onset. Can the OFF pathway drive non-image-forming visual behavior that tracks light offsets? To investigate this, we examined circadian photoentrainment, where mice confine their activity to nighttime immediately after light offset. It has been well established that outer retina photoreceptors, especially rods, are sufficient for circadian photoentrainment, but it is unknown whether circadian photoentrainment, which tracks sunrise and sunset, relies on visual information from the ON or OFF pathways in the retina.

We found that mGluR6; Opn4 dKO mice do not synchronize their circadian rhythms (free run) to 12 h light-12 h dark (12:12 LD) cycles (Figures 2E and 2F). Littermate control mice in 12:12 LD photoentrained to 24-h cycles as their period lengths become exactly 24 h (Figures 2D–2F). The period lengths of mGluR6; Opn4 dKO mice were largely unchanged in darkness (DD) and were comparable with controls (Figures 2F and S1). mGluR6 KO mice, which retain melanopsin expression, photoentrained to 12:12 LD cycles (Iwakabel et al., 1997; Figure S2), which is in agreement with findings showing that the intrinsic response of ipRGCs because of their expression of melanopsin is sufficient to drive circadian photoentrainment (Hattar et al., 2003; Panda et al., 2003). These results indicate that photoreceptor-mediated circadian photoentrainment requires a functional ON pathway and that the OFF pathway cannot drive this visually dependent behavior.

These results show that the ON pathway is required for photoreceptor contributions to at least two non-image-forming visual behaviors. This shows that the OFF pathway cannot compensate for the loss of the ON pathway to drive circadian photoentrainment or the PLR.

The OFF pathway drives an image-forming, visually guided behavioral task

The OFF pathway is thought to be capable of driving aspects of image-forming vision (Iwakabel et al., 1997; Morgans et al., 2009). However, mice in previous investigations of OFF pathway contributions to image-forming vision retained melanopsin, which is itself sufficient to drive some image-formation-dependent behaviors (Ecker et al., 2010). We set out to test whether our mGluR6; Opn4 dKO mice, which could not photoentrain and had no PLR, were functionally blind. We trained mice in an image-forming, visually guided behavioral task. Mice were trained to mark the presence of a photopic light stimulus (28,000 R*/rod/s) in one of two holes (Figure 2G). Littermate control mice, after training, complete this task correctly ~90% of the time (Figure 2H, blue circles). We find that mGluR6; Opn4 dKO mice complete this task comparable with control mice (Figure 2H, dark red circles). Therefore, at photopic light levels, the OFF pathway is sufficient for the animal to complete an image-forming, visually guided task, but the OFF pathway cannot drive two non-image-forming visual behaviors, the PLR and circadian photoentrainment.

The primary and secondary rod pathways drive the normal photopic PLR

After determining that only the ON pathway drives photoreceptor-mediated, non-image-forming vision, we investigated the precise contributions of rod and cone circuit pathways to the PLR using a different set of genetically modified mutant mouse lines. We first silenced the primary rod pathway by knocking out the presynaptic cell adhesion molecule Elfn1, which specifically prevents formation of the rod to RBC synapses (Figure 1C; Cao et al., 2015). Rod light responses in Elfn1 KO and littermate control mice were normal (Figure 1H). However, RBCs in Elfn1 KO mice did not respond to light flashes, indicating a lack of synaptic contact and signaling from rods to RBCs (Figure 1M; Cao et al., 2015). In contrast, ON and OFF CBC light responses in Elfn1 KO mice were normal (Figures 1R and 1W). Therefore, the Elfn1 mutation specifically silences signaling in the primary rod pathway (Cao et al., 2015). Using photopic light intensities, we observed that Elfn1 KO mice had no PLR deficits (Figures 3A and 3B), indicating that the primary rod pathway is dispensable for the normal photopic PLR.

To investigate whether the secondary rod pathway is required at photopic light levels for normal PLR, we used conditional cone-specific Cx36 KO (Cone-Cx36 KO) mice (Jin et al., 2020). Cx36 gap junctions are required to pass rod signals to cones (Figure 1D; Deans et al., 2002; Güldenagel et al., 2001). When recording from Cone-Cx36 KO mice, we found that rods show robust normal responses (Figure 1I). RBC responses in these mice were normal (Figure 1N). In agreement with the Cone-Cx36 mutation, at scotopic light levels, ON CBCs do not show responses, whereas OFF CBCs show responses with normal sensitivity (Figures 1S–1X; Asteriti et al., 2017; Deans et al., 2002; Güldenagel et al., 2001). Cone-Cx36 KO mice show a normal photopic PLR with the same kinetics as control mice (Figures 3A and 3B).

To silence the primary and secondary rod pathways, we generated Elfn1; Cx36 dKO mice (Figure 1E). Importantly, the cone pathways are unaffected in these mice (see blue circuit outlines in Figures 1E and 3G–3I). Rod light responses are normal in Elfn1; Cx36 dKO mice (Figure 1J). As predicted, light-evoked responses in RBCs and ON CBCs were absent (Figures 1O and 1T) at scotopic light levels. We recorded OFF CBC light responses in these mice, directly revealing the isolated tertiary rod pathway light response, without any input from the primary or secondary rod pathways (Figure 1Y; Table 1; Pang et al., 2012; Tsukamoto et al., 2001).

Remarkably, the PLR of Elfn1; Cx36 dKO mice is delayed with respect to light onset (Figures 3A–3C; ANOVA post hoc Dunnett's test, $p = 0.04$), in addition to a small pupil constriction deficit (Figure 3B). We quantified the delay by measuring the time to half-minimum pupil constriction. We find that Elfn1; Cx36 dKO mice show a delayed PLR compared with littermate controls (controls 2.6 ± 0.5 s and Elfn1; Cx36 dKO 5.9 ± 2.0 s to half constriction, ANOVA post hoc Dunnett's test, $p = 0.03$). Our data indicate that cone photoreceptor pathways, which are functional in the Elfn1; Cx36 dKO mouse (Figures 3G–3I), cannot drive the normal photopic PLR. The delayed response (Figure 3C) resembles the melanopsin-dependent PLR we observe in our mGluR6 KO animals (Figure 2C). The primary and secondary rod pathways can compensate for one another to drive a normal photopic PLR, but loss of both pathways results in PLR deficiencies.

Cone light responses cannot drive normal PLR but can drive image-forming vision

Our results in Elfn1; Cx36 dKO mice showing a PLR deficit indicate that functional cones (Figure 3G) cannot drive the normal photopic PLR even though we find that the secondary rod pathway, which routes rod light response signals through cone pathways, does drive the normal PLR. To understand why rod light responses, instead of cone light responses, are critical to a normal photopic PLR, we recorded from cone photoreceptors in retinal slices of Cone-Cx36 KO and their littermate control mice. Cone responses to photopic light flashes in control mice have a fast transient peak that decays into a smaller amplitude sustained response (Figure 3D, arrow). In Cone-Cx36 KO mice, the transient fast cone response is still present, but because cones are electrically isolated from rods, this response quickly decays to baseline (Figure 3E, arrow). Next we applied a background light of 332 R*/rod/s, which has been shown to suppress 80%–90% of the dark current in rods (Grimes et al., 2018b). We find that, in these light-adapted control mice, the cone response (Figure 3F, yellow trace) is comparable with the dark-adapted cone response in Cone-Cx36 KO mice (Figure 3F, cyan trace), showing that the sustained response in dark-adapted control cones (Figure 3F, blue trace) originates from rods. Thus, our data indicate that the rod-dependent sustained portion of the cone light response is necessary to drive a normal photopic PLR through the rod secondary pathway.

We find that cone pathways without rod input are unable to drive non-image-forming behavior, but we expect that cones can still drive aspects of image-forming vision. We examined this directly by adding a rod-suppressing background light (3,500 R*/rod/s) to the image-forming visual testing chamber to silence rod-dependent light responses (Figure 3J). Control mice were able to complete this behavioral task, indicating that cone light responses alone can drive this behavior (Figure 3K). To eliminate the potential for crosstalk in the outer retina photoreceptors, we used Cone-Cx36 KO mice to genetically uncouple rods and cones. Cone-Cx36 KO mice subjected to a rod-suppressing background light completed the task comparable with littermate control mice (Figure 3K). To genetically isolate the cone pathways from rods, we used Cx36 KO mice and Elfn1; Cx36 dKO mice. Cx36 KO mice and Elfn1; Cx36 dKO mice complete the visually guided behavioral task comparable with control mice (Figure 3K). These data indicate that cone light responses, without rod input, are sufficient to drive this image-forming, visually guided behavior, in direct contrast to our findings with the PLR.

Rod OFF pathways drive scotopic image-formation but do not drive the scotopic PLR

We next investigated how outer retinal circuits contribute to the PLR at dimmer light intensities. To study the contribution of the OFF pathway to the scotopic PLR, we measured the pupil constriction of mGluR6; Opn4 dKO mice in dim light (1 lux, 475 R*/rod/s). mGluR6; Opn4 dKO mice have no scotopic PLR (Figures 4A and 4B; one-way Student’s t test from dilation, $p = 0.2$). These results demonstrate that the rod tertiary pathway and rod secondary OFF pathway cannot drive the scotopic PLR. We find, however, that rod OFF pathways can drive image-forming vision. Dark-adapted mGluR6; Opn4 dKO mice were able to detect a dim light stimulus (~280 R*) in complete darkness and completed the visually guided behavioral task comparable with control mice (Figures 4C and 4D). Therefore, the rod secondary OFF or tertiary pathway can drive image formation.

The primary rod pathway is necessary and sufficient for the scotopic PLR

We then examined the rod pathway contributions to the scotopic PLR. In low light (1 lux, 475 R*/rod/s), we find a weak PLR with a large deficit in the Elfn1 KO mouse (Figures 5A and 5B). To investigate the role of the secondary rod pathway to the PLR in low light, we examined pupil constriction in Cone-Cx36 KO mice (Jin et al., 2020). Cone-Cx36 KO mice had indistinguishable pupil constriction at 1 lux compared with controls (Figures 5A and 5B). These results suggest that the secondary rod pathway is not required for the PLR at scotopic light levels. To determine whether the remaining pupil constriction in Elfn1 KO mice is due to the secondary pathway, we examined the scotopic PLR in Elfn1; Cx36 dKO mice. Silencing the primary and secondary rod pathways completely abolishes the scotopic PLR (Figures 5A and 5B). Therefore, although dispensable at photopic light levels, we find that the primary rod pathway is necessary for a normal PLR at scotopic light levels and that the secondary rod pathway cannot compensate for its loss.

For image-forming vision, the smallest photon capture events are thought to be conveyed by the primary rod pathway, which is more sensitive than the secondary and tertiary rod pathways (Table 1; Grimes et al., 2014; Ke et al., 2014). To investigate whether this difference in pathway contribution holds true for non-image-forming vision, we examined the PLR of Elfn1 KO mice and Cone-Cx36 KO mice at even lower light levels (0.1 lux, 73 R*/rod/s and 0.01 lux, 7 R*/rod/s). At 0.1 lux, Elfn1 KO mice have almost no PLR and show deficits compared with control mice (ANOVA, Dunnett, $p = 0.008$), whereas Cone-Cx36 KO mice show normal pupil constriction (ANOVA, Dunnett, $p = 0.98$) (Figures 5C and 5D). We observed a similar trend in the pupil constriction data at 0.01 lux (7 R*/rod/s), where Elfn1 KO animals show almost no pupil constriction (Figure 6B), but the constriction was not significantly different from controls, likely because of the limited constriction we see in controls at this dim light level. These results indicate that the primary rod pathway is the main driver behind the PLR at very low light levels. This demonstrates that, similar to image-forming vision, non-image-forming visual behavior requires the most sensitive retinal pathway for normal function.

DISCUSSION

Here we show that outer retinal circuit pathway contributions to non-image-forming and image-forming vision are distinct in surprising ways. We show that the outer retinal OFF pathway cannot drive circadian photoentrainment and the PLR, two non-image-forming, visually dependent behaviors, but is sufficient for driving image-forming, visually guided behaviors. We use a quantitative behavior, the PLR, to comprehensively define the outer retinal circuits driving non-image-forming vision over a wide range of light intensities. We find that the primary and secondary rod pathways drive the photopic PLR. Although the secondary pathway requires cone cells, the cone light responses, without rod input, are not able to drive non-image-forming vision despite driving image-forming vision. We find that the primary rod pathway is the only circuit necessary for the scotopic and mesopic PLR. Our results uncover vast differences between image-forming and non-image-forming vision in their OFF and photopic light responses. However, we also find similarities because the rod

primary pathway at scotopic light levels is the major circuit contributor to image-forming and non-image-forming vision.

The OFF pathway drives image-forming vision but not non-image-forming vision

We investigated the role of the OFF pathway in non-image-forming vision using mGluR6; Opn4 dKO mice. Circadian photoentrainment is a behavior that can encode light increments, decrements, or both. We find that the ON pathway is necessary for photoreceptor-mediated circadian photoentrainment. Remarkably, animals with a functional OFF pathway free run (lacking any circadian photoentrainment) even under light/dark conditions, similar to animals maintained under constant conditions. It has been shown previously, using mGluR6 KO mice, that the OFF pathway drives the PLR, a non-image-forming visual behavior, (Iwakabel et al., 1997). However, we showed in this study that the OFF pathway cannot drive the PLR and that the PLR is dependent on the outer retinal ON pathways for normal function. We showed that the remaining pupil constriction in mGluR6 KO mice is due to melanopsin because, in mGluR6; Opn4 dKO mice, all pupil constriction disappears. This is remarkable because we find that the OFF pathway is capable of driving an image-forming, visually guided behavioral task, indicating that the ON and OFF pathways do not play the same role in non-image-forming vision compared with image formation.

At this time, we can only speculate why and where in the circuitry this separation of the OFF pathway to the PLR and circadian photoentrainment occurs. It is also unknown whether this pathway separation is generalizable to other non-image-forming behaviors. Most non-image-forming visual behaviors, including the PLR, circadian photoentrainment, and the direct influence of light on sleep and mood, are thought to depend on M1 ipRGCs for normal function (Chen et al., 2011; Fernandez et al., 2018; Güler et al., 2008; Zhang et al., 2021), so it is tempting to conclude that the OFF pathway separation occurs in the retina. However, this conclusion ignores the fact that it is unknown whether other non-M1 ipRGCs and non-ipRGCs drive or modulate non-image-forming behaviors. Brain regions that play a central role in non-image-forming vision receive diverse ipRGC and non-ipRGC innervation (Baver et al., 2008; Beier et al., 2020; Quattrochi et al., 2019). The makeup of RGC innervation to non-image-forming brain regions will ultimately influence behavior; for example, genetically ablating the M1 ipRGC abolishes an animal's ability to photoentrain, but some PLR remains (Güler et al., 2008). Therefore, it is likely that there is some, but not complete, overlap in outer retinal circuit contributions that drive different non-image-forming visual behaviors. The diversity of ipRGC and non-ipRGC innervation to the olivary pretectal nucleus suggests that at least some OFF pathway separation from driving the PLR behavior occurs at the level of the thalamus rather than in the retina itself.

The rod-isolated cone light response is unable to drive a normal PLR

One of the controversies in the PLR field is whether the cone phototransduction pathway contributes to the PLR (Allen et al., 2011; Butler and Silver, 2011; Dkhissi-Benyahya et al., 2007; Hayter and Brown, 2018; Kostic et al., 2016; Lall et al., 2010). To isolate the cone light response, we used Elfn1; Cx36 dKO mice. Remarkably, these mice show a delay in their photopic PLR kinetics even though their cones are completely functional. The PLR in the Elfn1; Cx36 dKO mice resembles the PLR we observed in mGluR6 KO mice, which was

entirely due to melanopsin. Therefore, the fast kinetics of the PLR in single-pathway KO mice (Elfn1 KO and Cone-Cx36 KO) mice can only be attributed to rods (Cao et al., 2015; Deans et al., 2002; Keenan et al., 2016). This shows that the cone light response alone plays little to no role in driving the normal PLR.

In contrast, cone light responses drive image-forming vision. Mice with cones electrically isolated from rods (Cone-Cx36 KO) and subjected to a background rod-suppressing light were readily able to detect photopic light flashes. Therefore, cone light responses can drive image-forming vision but do not drive non-image-forming vision.

The primary and secondary rod pathways drive the photopic PLR

Our results show that the OFF pathway and rod-isolated cone light response are incapable of driving the PLR. The primary and secondary ON rod pathways drive the photoreceptor-mediated photopic PLR. Mice lacking the primary rod pathway (Elfn1 KO) retain a normal photopic PLR, indicating that the secondary ON rod pathway is sufficient to drive normal photopic pupil constriction (Figure 3B). When the secondary pathway is silenced (Cone-Cx36 KO), the PLR is also normal. Therefore, the rod to RBC synapse is sufficient for the fast photoreceptor-mediated photopic PLR (Figure 6A).

How do RBCs convey the signal to downstream circuitry to drive the photopic PLR? Although this is beyond the scope of this study, we speculated regarding the potential circuit pathways that might allow rods to drive M1 ipRGCs, the main light relays for the PLR and circadian photoentrainment (Güler et al., 2008; Lee et al., 2019; Weng et al., 2013; Zhao et al., 2014). There are at least three possibilities: (1) RBCs synapse directly onto M1 ipRGCs (Østergaard et al., 2007); (2) RBC signals are routed to M1 ipRGCs via the AII amacrine cell inhibitory glycinergic synapse, likely via another amacrine cell (Graydon et al., 2018; Newkirk et al., 2013; Pérez-Fernández et al., 2019; Reifler et al., 2015; Roy and Field, 2019; Sabbah et al., 2017, 2018; Tsukamoto and Omi, 2017); or (3) RBC signals are routed to M1 ipRGCs via the AII amacrine cell gap junction with Type 6 ON CBCs (Tsukamoto and Omi, 2017). Type 6 ON CBCs are the primary BC partner to M1 ipRGCs, making this a potential inner retinal circuit driving the PLR (Dumitrescu et al., 2009; Sabbah et al., 2018).

Non-image-forming vision requires the most sensitive retinal pathway for normal function

Electrophysiological evidence has suggested that ipRGCs receive light information from the primary rod pathway, but it has remained unknown whether this connection is behaviorally relevant (Weng et al., 2013). It has been shown more recently that the intrinsic melanopsin-dependent response is sensitive to scotopic light stimulation *ex vivo* (Lee et al., 2019), but the melanopsin contribution to the scotopic PLR is small (Keenan et al., 2016). We tested the behavioral relevance of the primary pathway directly by using Elfn1 KO mice and showed a clear pupil constriction deficit at low light levels (Figure 5D). Mice lacking the secondary rod pathway have no pupil constriction deficits at low light when the primary pathway is fully intact (Figure 5D). This shows that the primary rod pathway fully compensates for the secondary pathway at scotopic and mesopic light levels. The secondary pathway does not fully compensate for loss of the primary pathway (Figure 6B).

Our results show that the primary rod pathway is the predominate contributor to the scotopic and mesopic PLR (Figure 6A).

Limitations of the study

In this study, we used genetically modified mouse lines to dissect the retinal circuits driving visual behaviors *in vivo.* As in any study that uses mouse mutant lines, the possibility of unexpected changes that occur cannot be completely eliminated. For example, it is well known that retinal circuit pathways are highly interconnected; silencing one pathway can cause changes in another off-target pathway. Specifically, the Elfn1; Cx36 dKO mouse will also eliminate the gap junction in AII amacrine cells, which are key components of the rod primary pathway and important for network crosstalk (Deans et al., 2002). However, in our study, we carried out extensive electrophysiological recordings from all the mouse lines and showed that the major remaining components of each line are functional and can drive some aspects of vision.

Here, we investigated defined examples of divergent outer retinal circuitry driving three visually dependent behaviors (the PLR, circadian photoentrainment, and a visually guided behavioral task), but it is important to acknowledge the limits of generalizing our findings to all image- and non-image-forming visual behaviors. It is also important to clarify that the mGluR6; Opn4 dKO mice and Cx36 mutation mice we tested in the image-forming, visually guided behavioral task do not have completely normal vision. We use the visual task here to demonstrate that the remaining unsilenced retinal pathways in these mutant mice are functional at the image-formation behavioral level.

STAR★METHODS

RESOURCE AVAILABILITY

Lead contact—Further information and requests for resources and reagents should be directed to and will be fulfilled by the Lead Contact, Johan Pahlberg (johan.pahlberg@nih.gov).

Materials availability—This study did not generate new unique reagents.

Data and code availability—All data reported in this paper will be shared by the lead contact upon request. This paper does not report original code. Any additional information required to reanalyze the data reported in this paper is available from the lead contact upon request.

EXPERIMENTAL MODEL AND SUBJECT DETAILS

All mice were handled in accordance with guidelines of the Animal Care and Use Committees of the National Institute of Mental Health (NIMH). Male and female mice, aged 2 to 6 months, were used in experiments. mGluR6 KO were obtained from The Jackson Laboratory (Stock number 016883) (Maddox et al., 2008) and crossed with Opn4 knockout mice (Ecker et al., 2010) to obtain control mice (mGluR6+/−; Opn4 +/−) and double knockout mice (mGluR6−/−; Opn4 −/−), in addition to mGluR6 KO littermates

(mGluR6−/−; Opn4 +/−). Elfn1 KO mice (Cao et al., 2015) were crossed with Cx36 KO mice (a gift from the Dr. Jeffrey Diamond laboratory) (Deans et al., 2001) to generate control mice (Elfn1 +/+; Cx36 +/+), Elfn1 KO mice (Elfn1 −/−; Cx36 +/+), and Elfn1; Cx36 double knockout mice (Elfn1 −/−; Cx36 −/−). Cone-Cx36 KO mice (Cx36 fl/fl; HRGP Cre/+) are described in (Jin et al., 2020). Both Cx36 fl/fl; HRGP +/+ and Cx36 +/+; HRGP Cre/+ were used as littermate control mice. Mice were group housed in a temperature and humidity controlled room under a 12 h light-dark cycle with light intensity near 100 lux. Food and water were available *ad libitum*.

METHOD DETAILS

Single-cell electrophysiological recordings—Light-evoked responses were made from dark-adapted retinal slices as previously described (Pahlberg et al., 2017). Briefly, mice were dark adapted overnight and euthanized according to protocols and guidelines approved by NIH. Their eyes were enucleated and hemisected under infrared light. Retinas were extracted from the eye cups, embedded in low density agar gel (3%) and cut with a vibratome to obtain 200 μm thick slices. Retina slices were perfused with Ames' medium with an 8 mL/min flow rate (equilibrated with 5% CO_2/ 95% O_2), maintained at 35–37°C, and visualized in the infrared. The pipette internal solution for whole-cell patch clamp recordings contained (in mM): 125 K-aspartate, 10 KCl, 10 HEPES, 5 N-methyl glucamine-HEDTA, 0.5 CaCl2, 1 ATP-Mg and 0.2 GTP-Mg; pH was adjusted to 7.4 with NMG-OH. Light responses were generated delivering 20 ms flashes from a blue-green light emitting diode (λ_{max} ~ 505 nm). Flash strengths were varied from a just-measurable response to those that produced a maximal response, increasing in factors of two. Membrane currents were filtered at 300 Hz and sampled at 10 kHz. Light sensitivity for each cell type was estimated from the half-maximal flash strength from the best Hill fit, for each genotype. To identify RBCs, ON CBCs, and OFF CBCs the shape and morphology of the cells, the time course, the amplitude and the polarity of their light responses were considered. As a control, the electrode internal solution for some experiments contained Alexa 750 (100 μM), which allowed visualization of the cells in the far red without significantly bleaching the visual pigment (see Figure S3). The subtypes of ON and OFF CBCs were not characterized. All recordings were performed between circadian time 4 and 12. Multiple cell types were recorded from the same slice, typically no more than 50 μm apart from each other. In Figure 3, the capacitance for cones was 8 ± 0.5 pF (n = 5) in control and 8.6 ± 1.1 pF for Cone-Cx36 KO mice (n = 4), the rod capacitance was 3.5 ± 0.2 pF (n = 5) for control and 4.6 ± 0.4 pF (n = 8) for Cone-Cx36 KO mice.

Pupillometry—The pupillary light response (PLR) experiments were performed as previously described (Keenan et al., 2016). Briefly, mice were handled prior to PLR experiment days to habituate animals to handling. On the day of the experiment, mice were dark adapted for at least 1 h before being scruffed and placed in front of a fixed-focus video camera (Sony 4K HD Camcorder FDRAX3) under infrared light (ICAMI IR Illuminators, λ = 850 nm). The dark-adapted pupils were recorded for at least 5 s before turning the stimulus light on. The stimulus light bulb (Sunlite 6500K A19/LED/10W) was placed directly above the mouse such that the stimulus provided 100 lux light as measured by a lux meter (EXTECH Foot Candle/Lux Light Meter, 401025). For experiments under scotopic

conditions, neutral density filters were placed over the light to achieve 1, 0.1 and 0.01 lux stimuli. Light levels were converted to R*/rod/sec by measuring the spectrum of the light source with different ND filters in place and converted as described in these references (Jacobs and Williams, 2007; Lyubarsky et al., 2004; Pasquale et al., 2020). Pupils were recorded for at least 30 s following light onset. All recordings were performed between Zeitgeber times 4 and 12.

A semi-automated custom script was used to measure the pupil area in every video frame (30 frames/second) and binned every 2 s to generate the pupil traces over time. For each mouse, all measurements were normalized to the average dark-adapted pupil size across the 5 s immediately prior to light onset. The minimum pupil diameter measurement is the minimum pupil area averaged over 10 frames for each mouse. Dark-adapted pupil areas did not differ between mutant and control mice (ANOVA post hoc Dunnett's method, $p > 0.5$ between mutant mouse lines and controls, Figure S4). Minimum pupil area (maximum pupil constriction) was taken from pupil measurements between $t = 0$ to 30 s after light onset.

Wheel-running activity—Mice were housed individually in cages with a 4.5 inch wheel and their activity was measured by wheel rotations collected in 5-min bins with VitalView software (MiniMitter; Respironics). Mice were placed in 12 h light – 12 h dark (12:12 LD) cycles at ~700 lux for at least 2 weeks, followed by darkness (DD) for 2–3 weeks, and placed in 12:12 LD again for 2 weeks. Custom MATLAB scripts were used to generate actograms and measure activity onset to calculate period lengths. The wheel running activity of mice exposed to changing light paradigms is recorded in 5-min bins double plotted.

Two Alternative Forced Choice Paradigm—Visually guided behavior was tested using a novel Two Alternative Forced Choice Paradigm. The mice were trained to react to a light stimulus in one of two nose-poke holes in a modified 9-hole behavioral box (Humby et al., 2005). Mice were handled and weighed for two days prior to training to habituate, after which they were put on food restriction and maintained at 80% or greater bodyweight. Each training session was 60 min or 30 correct trials long, whichever came first.

In the first phase of training, mice were taught to associate the food-hopper with reward pellets. The food-hopper was initially baited with 4 pellets (2 pellets on day 2, 1 pellet on day 3), and every 40 s (60 s on day 2, 60 s on day 3). Reward pellets were automatically dispensed.

Next, mice were trained to associate a 505 nm light stimulus with the reward. First, both holes were baited with an 8% sucrose solution and crushed pellets, and a stimulus tone preceded both holes lighting up. The mouse was required to poke either hole to trigger the reward tone and pellet. Next, the light stimulus was restricted to one hole, staying on until the mouse poked the correct hole. The mice had to cross an infrared beam in front of the holes to trigger the beginning of a trial and reach 80% accuracy for two consecutive days to advance to the testing phase.

In the testing phase the light stimulus illuminated only one hole for 1–16 s. If at the end of a stimulus there was no response by the mouse, the trial was counted as an omission. The

accuracy for the different strains (Fractional Correct) was calculated by dividing the correct trials by the total number of trials in the session (correct, incorrect, premature, omissions).

QUANTIFICATION AND STATISTICAL ANALYSIS

Statistical analyses are listed in the text and Figure legends. Number of animals (n) used are indicated in the Figures, Figure legends and Table 1. Figures display values for individual animals and error bars that indicate the standard error of the mean (SEM). The statistical analyses used throughout the paper include ANOVA and the Student's t test and assume the measurement distributions are normal. All analyses were done in Microsoft Excel and MATLAB using built in functions.

Supplementary Material

Refer to Web version on PubMed Central for supplementary material.

ACKNOWLEDGMENTS

This project was supported in part by funding from the Intramural Research Programs of the NIDCR, NINDS, and NEI at the National Institutes of Health (to J.P.), funding from NIMH project MH002964 (to S.H.), and in part by the NIMH IRP Rodent Behavioral Core (MH002952). We thank Dr. Hui Wang in the Hattar lab for management of the *Opn4*^{Cre} mouse line, Dr. Hua Tian in the Dr. Jeff Diamond lab for management of the Cx36 knockout line shared with us, and Dr. Sean Bradley for technical assistance with vision behavior experiments.

REFERENCES

Allen AE, Brown TM, and Lucas RJ (2011). A distinct contribution of short-wavelength-sensitive cones to light-evoked activity in the mouse pretectal olivary nucleus. J. Neurosci 31, 16833–16843. 10.1523/JNEUROSCI.2505-11.2011. [PubMed: 22090509]

Altimus CM, Güler AD, Alam NM, Arman AC, Prusky GT, Sampath AP, and Hattar S (2010). Rod photoreceptors drive circadian photoentrainment across a wide range of light intensities. Nat. Neurosci 13, 1107–1112. 10.1038/nn.2617. [PubMed: 20711184]

Ashmore JF, and Copenhagen DR (1980). Different postsynaptic events in two types of retinal bipolar cell. Nature 288, 84–86. 10.1038/288084a0. [PubMed: 6253819]

Asteriti S, Gargini C, and Cangiano L (2014). Mouse rods signal through gap junctions with cones. Elife 3, e01386. 10.7554/eLife.01386. [PubMed: 24399457]

Asteriti S, Gargini C, and Cangiano L (2017). Connexin 36 expression is required for electrical coupling between mouse rods and cones. Vis. Neurosci 34, E006. 10.1017/S0952523817000037. [PubMed: 28965521]

Baver SB, Pickard GE, Sollars PJ, and Pickard GE (2008).Two types of melanopsin retinal ganglion cell differentially innervate the hypothalamic suprachiasmatic nucleus and the olivary pretectal nucleus. Eur. J. Neurosci 27, 1763–1770. 10.1111/j.1460-9568.2008.06149.x. [PubMed: 18371076]

Beier C, Zhang Z, Yurgel M, and Hattar S (2020). Projections of ipRGCs and conventional RGCs to retinorecipient brain nuclei. J. Comp. Neurol 529, 1863–1875. 10.1002/cne.25061. [PubMed: 33104235]

Butler MP, and Silver R (2011). Divergent photic thresholds in the non-image-forming visual system: entrainment, masking and pupillary light reflex. Proc. Biol. Sci 278, 745–750. 10.1098/rspb.2010.1509. [PubMed: 20861055]

Cao Y, Pahlberg J, Sarria I, Kamasawa N, Sampath AP, and Martemyanov KA (2012). Regulators of G protein signaling RGS7 and RGS11 determine the onset of the light response in on bipolar neurons. Proc. Natl. Acad. Sci. USA 109, 7905–7910. 10.1073/pnas.1202332109. [PubMed: 22547806]

Cao Y, Sarria I, Fehlhaber KE, Kamasawa N, Orlandi C, James KN, Hazen JL, Gardner MR, Farzan M, Lee A, et al. (2015). Mechanism for selective synaptic wiring of rod photoreceptors into

the retinal circuitry and its role in vision. Neuron 87, 1248–1260. 10.1016/j.neuron.2015.09.002. [PubMed: 26402607]

Chen S-K, Badea TC, and Hattar S (2011). Photoentrainment and pupillary light reflex are mediated by distinct populations of ipRGCs. Nature 476, 92–95. 10.1038/nature10206. [PubMed: 21765429]

Dacheux RF, and Raviola E (1982). Horizontal cells in the retina of the rabbit. J. Neurosci 2, 1486–1493. 10.1523/jneurosci.02-10-01486.1982. [PubMed: 6181232]

Dacheux RF, and Raviola E (1986). The rod pathway in the rabbit retina: a depolarizing bipolar and amacrine cell. J. Neurosci 6, 331–345. 10.1523/jneurosci.06-02-00331.1986. [PubMed: 3950701]

Deans MR, Gibson JR, Sellitto C, Connors BW, and Paul DL (2001). Synchronous activity of inhibitory networks in neocortex requires electrical synapses containing connexin36. Neuron 31, 477–485. 10.1016/S0896-6273(01)00373-7. [PubMed: 11516403]

Deans MR, Volgyi B, Goodenough DA, Bloomfield SA, and Paul DL (2002). Connexin36 is essential for transmission of rod-mediated visual signals in the mammalian retina. Neuron 36, 703–712. 10.1016/s0896-6273(02)01046-2. [PubMed: 12441058]

Demb JB, and Singer JH (2012). Intrinsic properties and functional circuitry of the All amacrine cell. Vis. Neurosci 29, 51–60. 10.1017/S0952523811000368. [PubMed: 22310372]

Demb JB, and Singer JH (2015). Functional circuitry of the retina. Annu. Rev. Vis. Sci 1, 263–289. 10.1146/annurev-vision-082114-035334. [PubMed: 28532365]

DeVries SH, and Baylor DA (1995). An alternative pathway for signal flow from rod photoreceptors to ganglion cells in mammalian retina. Proc. Natl. Acad. Sci. USA 92, 10658–10662. 10.1073/pnas.92.23.10658. [PubMed: 7479860]

Dkhissi-Benyahya O, Gronfier C, De Vanssay W, Flamant F, and Cooper HM (2007). Modeling the role of mid-wavelength cones in circadian responses to light. Neuron 53, 677–687. 10.1016/j.neuron.2007.02.005. [PubMed: 17329208]

Dumitrescu ON, Pucci FG, Wong KY, and Berson DM (2009). Ectopic retinal ON bipolar cell synapses in the OFF inner plexiform layer: contacts with dopaminergic amacrine cells and melanopsin ganglion cells. J. Comp. Neurol 517, 226–244. 10.1002/cne.22158. [PubMed: 19731338]

Ecker JL, Dumitrescu ON, Wong KY, Alam NM, Chen S-K, LeGates T, Renna JM, Prusky GT, Berson DM, and Hattar S (2010). Melanopsin-expressing retinal ganglion-cell photoreceptors: cellular diversity and role in pattern vision. Neuron 67, 49–60. 10.1016/J.NEURON.2010.05.023. [PubMed: 20624591]

Euler T, and Masland RH (2000). Light-evoked responses of bipolar cells in a mammalian retina. J. Neurophysiol 83,1817–1829. 10.1152/jn.2000.83.4.1817. [PubMed: 10758094]

Fernandez DC, Fogerson PM, Lazzerini Ospri L, Thomsen MB, Layne RM, Severin D, Zhan J, Singer JH, Kirkwood A, Zhao H, et al. (2018). Light affects mood and learning through distinct retina-brain pathways. Cell 175, 71–84.e18. 10.1016/j.cell.2018.08.004. [PubMed: 30173913]

Field GD, and Rieke F (2002). Nonlinear signal transfer from mouse rods to bipolar cells and implications for visual sensitivity. Neuron 34, 773–785. 10.1016/S0896-6273(02)00700-6. [PubMed: 12062023]

Graydon CW, Lieberman EE, Rho N, Briggman KL, Singer JH, and Diamond JS (2018). Synaptic transfer between rod and cone pathways mediated by All amacrine cells in the mouse retina. Curr. Biol 28, 2739–2751.e3. 10.1016/j.cub.2018.06.063. [PubMed: 30122532]

Grimes WN, Schwartz GW, and Rieke F (2014). The synaptic and circuit mechanisms underlying a change in spatial encoding in the retina. Neuron 82, 460–473. 10.1016/j.neuron.2014.02.037. [PubMed: 24742466]

Grimes WN, Songco-Aguas A, and Rieke F (2018a). Parallel processing of rod and cone signals: retinal function and human perception. Annu. Rev. Vis. Sci 4, 123–141. 10.1146/annurev-vision-091517-034055. [PubMed: 29883274]

Grimes WN, Baudin J, Azevedo AW, and Rieke F (2018b). Range, routing and kinetics of rod signaling in primate retina. Elife 7, 1–21. 10.7554/eLife.38281.

Güldenagel M, Ammermüller J, Feigenspan A, Teubner B, Degen J, Söhl G, Willecke K, and Weiler R (2001). Visual transmission deficits in mice with targeted disruption of the gap junction

gene connexin36. J. Neurosci 21, 6036–6044. 10.1523/jneurosci.21-16-06036.2001. [PubMed: 11487627]

Güler AD, Ecker JL, Lall GS, Haq S, Altimus CM, Liao H-W, Barnard AR, Cahill H, Badea TC, Zhao H, et al. (2008). Melanopsin cells are the principal conduits for rod–cone input to non-image-forming vision. Nature 453, 102–105. 10.1038/nature06829. [PubMed: 18432195]

Hattar S, Lucas RJ, Mrosovsky N, Thompson S, Douglas RH, Hankins MW, Lem J, Biel M, Hofmann F, Foster RG, and Yau KW (2003). Melanopsin and rod–cone photoreceptive systems account for all major accessory visual functions in mice. Nature 424, 75–81. 10.1038/nature01761.

Hayter EA, and Brown TM (2018). Additive contributions of melanopsin and both cone types provide broadband sensitivity to mouse pupil control. BMC Biol. 16, 83. 10.1186/s12915-018-0552-1. [PubMed: 30064443]

Humby T, Wilkinson L, and Dawson G (2005). Assaying aspects of attention and impulse control in mice using the 5-choice serial reaction time task. Curr. Protoc. Neurosci 31. 10.1002/0471142301.ns0805hs31.

Iwakabel H, Katsuura G, Ishibash C, and Nakanishil S (1997). Impairment of pupillary responses and optokinetic nystagmus in the mGluR6-deficient-Mouse. Neuropharmacology 36, 135–143. 10.1016/s0028-3908(96)00167-0. [PubMed: 9144650]

Jacobs GH, and Williams GA (2007). Contributions of the mouse UV photopigment to the ERG and to vision. Doc. Ophthalmol 115, 137–144. 10.1007/s10633-007-9055-z. [PubMed: 17479214]

Jin N, Zhang Z, Keung J, Youn SB, Ishibashi M, Tian L-M, Marshak DW, Solessio E, Umino Y, Fahrenfort I, et al. (2020). Molecular and functional architecture of the mouse photoreceptor network. Sci. Adv 6, eaba7232. https://www.science.org/doi/10.1126/sciadv.aba7232. [PubMed: 32832605]

Ke JB, Wang YV, Borghuis BG, Cembrowski MS, Riecke H, Kath WL, Demb JB, and Singer JH (2014). Adaptation to background light enables contrast coding at rod bipolar cell synapses. Neuron 81, 388–401. 10.1016/j.neuron.2013.10.054. [PubMed: 24373883]

Keenan WT, Rupp AC, Ross RA, Somasundaram P, Hiriyanna S, Wu Z, Badea TC, Robinson PR, Lowell BB, and Hattar SS (2016). A visual circuit uses complementary mechanisms to support transient and sustained pupil constriction. Elife 5, 1–23. 10.7554/eLife.15392.

Kostic C, Crippa SV, Martin C, Kardon RH, Biel M, Arsenijevic Y, and Kawasaki A (2016). Determination of rod and cone influence to the early and late dynamic of the pupillary light response. Invest. Ophthalmol. Vis. Sci 57, 2501–2508. 10.1167/iovs.16-19150. [PubMed: 27152964]

Lall GS, Revell VL, Momiji H, Al Enezi J, Altimus CM, Güler AD, Aguilar C, Cameron MA, Allender S, Hankins MW, and Lucas RJ (2010). Distinct contributions of rod, cone, and melanopsin photoreceptors to encoding irradiance. Neuron 66, 417–428. 10.1016/j.neuron.2010.04.037. [PubMed: 20471354]

Lee SK, Sonoda T, and Schmidt TM (2019). M1 intrinsically photosensitive retinal ganglion cells integrate rod and melanopsin inputs to signal in low light. Cell Rep. 29, 3349–3355.e2. 10.1016/j.celrep.2019.11.024. [PubMed: 31825819]

Li W, Keung JW, and Massey SC (2004). Direct synaptic connections between rods and OFF cone bipolar cells in the rabbit retina. J. Comp. Neurol 474, 1–12. 10.1002/cne.20075. [PubMed: 15156575]

Lucas RJ, Douglas RH, and Foster RG (2001). Characterization of an ocular photopigment capable of driving pupillary constriction in mice. Nat. Neurosci 4, 621–626. 10.1038/88443. [PubMed: 11369943]

Lucas RJ, Hattar S, Takao M, Berson DM, Foster RG, and Yau KW (2003). Diminished pupillary light reflex at high irradiances in melanopsin-knockout mice. Science 299, 245–247. 10.1126/science.1077293. [PubMed: 12522249]

Lyubarsky AL, Daniele LL, and Pugh EN (2004). From candelasto photo-isomerizations in the mouse eye by rhodopsin bleaching in situ and the light-rearing dependence of the major components of the mouse ERG. Vis. Res 44, 3235–3251. 10.1016/j.visres.2004.09.019. [PubMed: 15535992]

Maddox DM, Vessey KA, Yarbrough GL, Invergo BM, Cantrell DR, Inayat S, Balannik V, Hicks WL, Hawes NL, Byers S, et al. (2008). Allelic variance between GRM6 mutants, Grm6nob3

and Grm6nob4 results in differences in retinal ganglion cell visual responses. J. Physiol 586, 4409–4424. [PubMed: 18687716]

Masland RH (2012). The neuronal organization of the retina. Neuron 76, 266–280. 10.1016/j.neuron.2012.10.002. [PubMed: 23083731]

Masu M, Iwakabe H, Tagawa Y, Miyoshi T, Yamashita M, Fukuda Y, Sasaki H, Hiroi K, Nakamura Y, Shigemoto R, et al. (1995). Specific deficit of the ON response in visual transmission by targeted disruption of the mGluR6 gene. Cell 80, 757–765. [PubMed: 7889569]

Morgans CW, Zhang J, Jeffrey BG, Nelson SM, Burke NS, Duvoisin RM, and Brown RL (2009). TRPM1 is required for the depolarizing light response in retinal ON-bipolar cells. Proc. Natl. Acad. Sci. USA 106, 19174–19178. 10.1073/pnas.0908711106. [PubMed: 19861548]

Mrosovsky N, and Hattar S (2003). Impaired masking responses to light in melanopsin-knockout mice. Chronobiol. Int 20, 989–999. 10.1081/CBI-120026043. [PubMed: 14680139]

Nakajima Y, Iwakabe H, Akazawa C, Nawa H, Shigemoto R, Mizuno N, and Nakanishi S (1993). Molecular characterization of a novel retinal metabotropic glutamate receptor mGluR6 with a high agonist selectivity for L-2-amino-4-phosphonobutyrate. J. Biol. Chem 268, 11868–11873. 10.1016/s0021-9258(19)50280-0. [PubMed: 8389366]

Nelson R (1977). Cat cones have rod input: a comparison of the response properties of cones and horizontal cell bodies in the retina of the cat. J. Comp. Neurol 172, 109–135. 10.1002/cne.901720106. [PubMed: 838876]

Newkirk GS, Hoon M, Wong RO, and Detwiler PB (2013). Inhibitory inputs tune the light response properties of dopaminergic amacrine cells in mouse retina. J. Neurophysiol 110, 536–552. 10.1152/jn.00118.2013. [PubMed: 23636722]

Nomura A, Shigemoto R, Nakamura Y, Okamoto N, Mizuno N, and Nakanishi S (1994). Developmentally regulated postsynaptic localization of a metabotropic glutamate receptor in rat rod bipolar cells. Cell 77, 361–369. 10.1016/0092-8674(94)90151-1. [PubMed: 8181056]

Okawa H, Miyagishima KJ, Arman AC, Hurley JB, Field GD, and Sampath AP (2010). Optimal processing of photoreceptor signals is required to maximize behavioural sensitivity. J. Physiol 588, 1947–1960. 10.1113/jphysiol.2010.188573. [PubMed: 20403975]

Østergaard J, Hannibal J, and Fahrenkrug J. (2007). Synaptic contact between melanopsin-containing retinal ganglion cells and rod bipolar cells. Invest. Ophthalmol. Vis. Sci 48, 3812. 10.1167/iovs.06-1322. [PubMed: 17652756]

Pahlberg J, Frederiksen R, Pollock GE, Miyagishima KJ, Sampath AP, and Cornwall MC (2017). Voltage-sensitive conductances increase the sensitivity of rod photoresponses following pigment bleaching. J. Physiol 595, 3459–3469. 10.1113/JP273398. [PubMed: 28168711]

Panda S, Sato TK, Castrucci AM, Rollag M, DeGrip WJ, DeGrip W, Hogenesch JB, Hogenesch J, Provencio I, Kay SA, and Kay S (2002). Melanopsin (Opn4) requirement for normal light-induced circadian phase shifting. Science 298, 2213–2216. 10.1126/science.1076848. [PubMed: 12481141]

Panda S, Provencio I, Tu DC, Pires SS, Rollag MD, Castrucci AM, Pletcher MT, Sato TK, Wiltshire T, Andahazy M, et al. (2003). Melanopsin is required for non-image-forming photic responses in blind mice. Science 301, 525–527. 10.1126/science.1086179. [PubMed: 12829787]

Pang JJ, Gao F, Paul DL, and Wu SM (2012). Rod, M-cone and M/Scone inputs to hyperpolarizing bipolar cells in the mouse retina. J. Physiol 590, 845–854. 10.1113/jphysiol.2011.224113. [PubMed: 22219344]

Pasquale R, Umino Y, and Solessio E (2020). Rod photoreceptors signal fast changes in daylight levels using a CX36-independent retinal pathway in mouse. J. Neurosci 40, 796–810. 10.1523/JNEUROSCI.0455-19.2019. [PubMed: 31776212]

Pérez-Fernández V, Milosavljevic N, Allen AE, Vessey KA, Jobling AI, Fletcher EL, Breen PP, Morley JW, and Cameron MA (2019). Rod photoreceptor activation alone defines the release of dopamine in the retina. Curr. Biol 29, 763–774.e5. 10.1016/j.cub.2019.01.042. [PubMed: 30799247]

Quattrochi LE, Stabio ME, Kim I, Ilardi MC, Michelle Fogerson P, Leyrer ML, and Berson DM (2019). The M6 cell: a small-field bistratified photosensitive retinal ganglion cell. J. Comp. Neurol 527, 297–311. 10.1002/cne.24556. [PubMed: 30311650]

Reifler AN, Chervenak AP, Dolikian ME, Benenati BA, Li BY, Wachter RD, Lynch AM, Demertzis ZD, Meyers BS, Abufarha FS, et al. (2015). All spiking, sustained ON displaced amacrine cells

receive gap-junction input from melanopsin ganglion cells. Curr. Biol 25, 2763–2773. 10.1016/j.cub.2015.09.018. [PubMed: 26441349]

Roy S, and Field GD (2019). Dopaminergic modulation of retinal processing from starlight to sunlight. J. Pharmacol. Sci 140, 86–93. 10.1016/j.jphs.2019.03.006. [PubMed: 31109761]

Sabbah S, Berg D, Papendorp C, Briggman KL, and Berson DM (2017). A Cre mouse line for probing irradiance- and direction-encoding retinal networks. eNeuro 4, ENEURO.0065-17.2017. 10.1523/ENEURO.0065-17.2017.

Sabbah S, Papendorp C, Koplas E, Beltoja M, Etebari C, Gunesch AN, Carrete L, Kim MT, Manoff G, Bhatia-Lin A, et al. (2018). Synaptic circuits for irradiance coding by intrinsically photosensitive retinal ganglion cells. Preprint at bioRxiv. http://biorxiv.org/lookup/doi/10.1101/442954.

Tsukamoto Y, and Omi N (2017). Classification of mouse retinal bipolar cells: type-specific connectivity with special reference to rod-driven All amacrine pathways. Front. Neuroanat 11, 92. 10.3389/fnana.2017.00092. [PubMed: 29114208]

Tsukamoto Y, Morigiwa K, Ueda M, and Sterling P (2001). Microcircuits for night vision in mouse retina. J. Neurosci 21, 8616–8623. 10.1523/jneurosci.21-21-08616.2001. [PubMed: 11606649]

van Oosterhout F, Fisher SP, van Diepen HC, Watson TS, Houben T, VanderLeest HT, Thompson S, Peirson SN, Foster RG, and Meijer JH (2012). Ultraviolet light provides a major input to non-image-forming light detection in mice. Curr. Biol 22, 1397–1402. 10.1016/j.cub.2012.05.032. [PubMed: 22771039]

Völgyi B, Deans MR, Paul DL, and Bloomfield SA (2004). Convergence and segregation of the multiple rod pathways in mammalian retina. J. Neurosci 24, 11182–11192. 10.1523/JNEUROSCI.3096-04.2004. [PubMed: 15590935]

Weng S, Estevez ME, and Berson DM (2013). Mouse ganglion-cell photoreceptors are driven by the most sensitive rod pathway and by both types of cones. PLoS One 8, e66480. 10.1371/journal.pone.0066480. [PubMed: 23762490]

Xu Y, Dhingra A, Fina ME, Koike C, Furukawa T, and Vardi N (2012). mGluR6 deletion renders the TRPM1 channel in retina inactive. J. Neurophysiol 107, 948–957. 10.1152/jn.00933.2011. [PubMed: 22131384]

Zhang Z, Beier C, Weil T, and Hattar S (2021). The retinal ipRGC-preoptic circuit mediates the acute effect of light on sleep. Nat. Commun 12, 5115. 10.1038/s41467-021-25378-w. [PubMed: 34433830]

Zhao X, Stafford BK, Godin AL, King WM, and Wong KY (2014). Photoresponse diversity among the five types of intrinsically photosensitive retinal ganglion cells: light responses of melanopsin ganglion cells. J. Physiol 592, 1619–1636. 10.1113/jphysiol.2013.262782. [PubMed: 24396062]

Highlights

- The OFF pathway drives image-forming vision but not non-image-forming vision
- Non-image-forming vision requires the most sensitive retinal pathway
- The primary rod pathway is necessary and sufficient for the pupillary light response
- The primary and secondary rod pathways drive the photopic pupillary light response

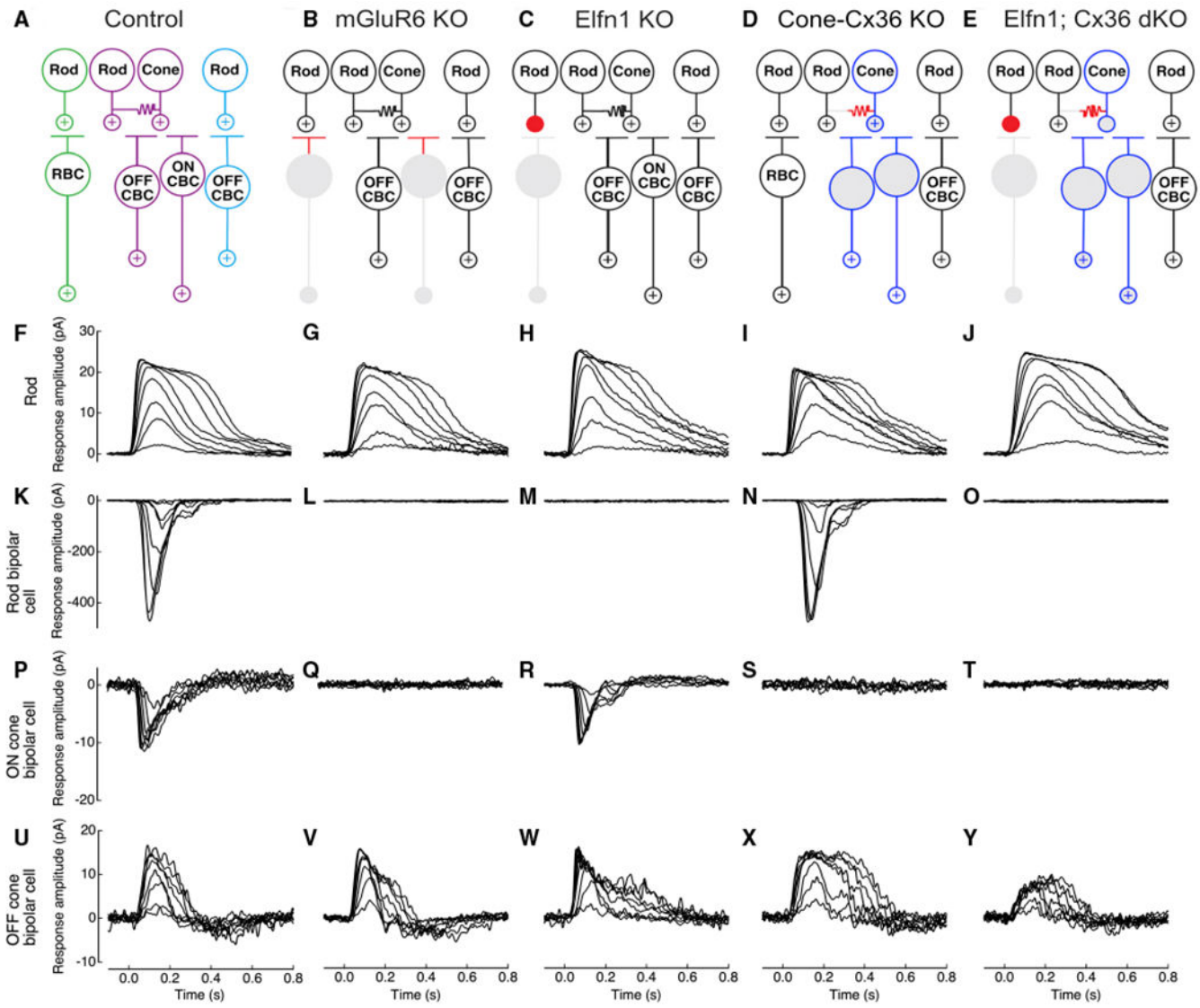

Figure 1. Rod and cone circuit pathways in control and mutant mice

(A) A schematic of the three rod pathways in the mammalian outer retina. In the primary rod pathway (green), the rod signal is passed from rods to rod BCs (RBCs). In the secondary rod pathway (purple), the rod signal is passed from rods to cones via a gap junction connection and then from cones to ON and OFF cone BCs (CBCs). In the tertiary rod pathway (blue), the rod signal is passed from rods to OFF CBCs.

(B) A retinal circuit schematic of the mGluR6 knockout (KO) mouse showing functional and non-functional pathways. RBCs and ON CBCs cannot receive glutamate signals because of loss of metabotropic glutamate receptor 6 (mGluR6) at their dendrites (red). The downstream rod ON pathways no longer receive rod input (gray).

(C) A retinal circuit schematic of the Elfn1 KO mouse. Because of loss of the presynaptic protein Elfn1, the synapse between rods and RBCs is non-functional (red). The primary pathway no longer receives rod input (gray).

(D) A retinal circuit schematic of the Cone-Cx36 KO mouse. Because of loss of connexin 36 (Cx36) in cones, no gap junctions are formed between rods and cones (red). The secondary pathway no longer receives direct rod input (gray); indirect input from the primary rod pathway via the All amacrine cell (not pictured) is still functional (white synapses). Cone pathways, indicated by blue outlines, are functional.

(E) A retinal circuit schematic of the Elfn1; Cx36 double KO (dKO) mouse. The synapse between the rod and RBC is non-functional, and there is lack of rod-to-cone gap-junctional coupling (red). The primary and secondary rod pathways no longer receive rod input (gray). Cone pathways, indicated by blue outlines, are functional.

(F–J) Physiological recordings of rod photocurrents in retinal slices from control, mGluR6 KO, Elfn1 KO, Cone-Cx36 KO, and Elfn1; Cx36 dKO mice, respectively. Recordings were made in whole-cell patch-clamp mode (V_m = −40 mV). 20-ms light flashes were given at time 0 s. Flash strength ranged from 2.5–156 R*/rod. Recordings are representative of data collected across several cells (Table 1).

(K–O) Physiological recordings of light-evoked RBC responses. Recordings were made in the same slices as the rod recordings and as before, with some differences (V_m = −60 mV and flash strength from 0.2–16 R*/rod). RBC light responses were never observed in mGluR6 KO, Elfn1 KO, or Elfn1; Cx36 dKO mice (Table 1; Figure S3).

(P–T) ON CBC responses as described for RBCs. Flash strength spanned a range expected to activate the primary and secondary rod pathways. ON CBC light responses were never observed in mGluR6 KO, Cone-Cx36 KO, or Elfn1; Cx36 dKO mice (Table 1; Figure S3).

(U–Y) OFF CBCs responses as described for ON CBCs. Flash strength spanned a range expected to activate the primary, secondary, and tertiary rod pathways.

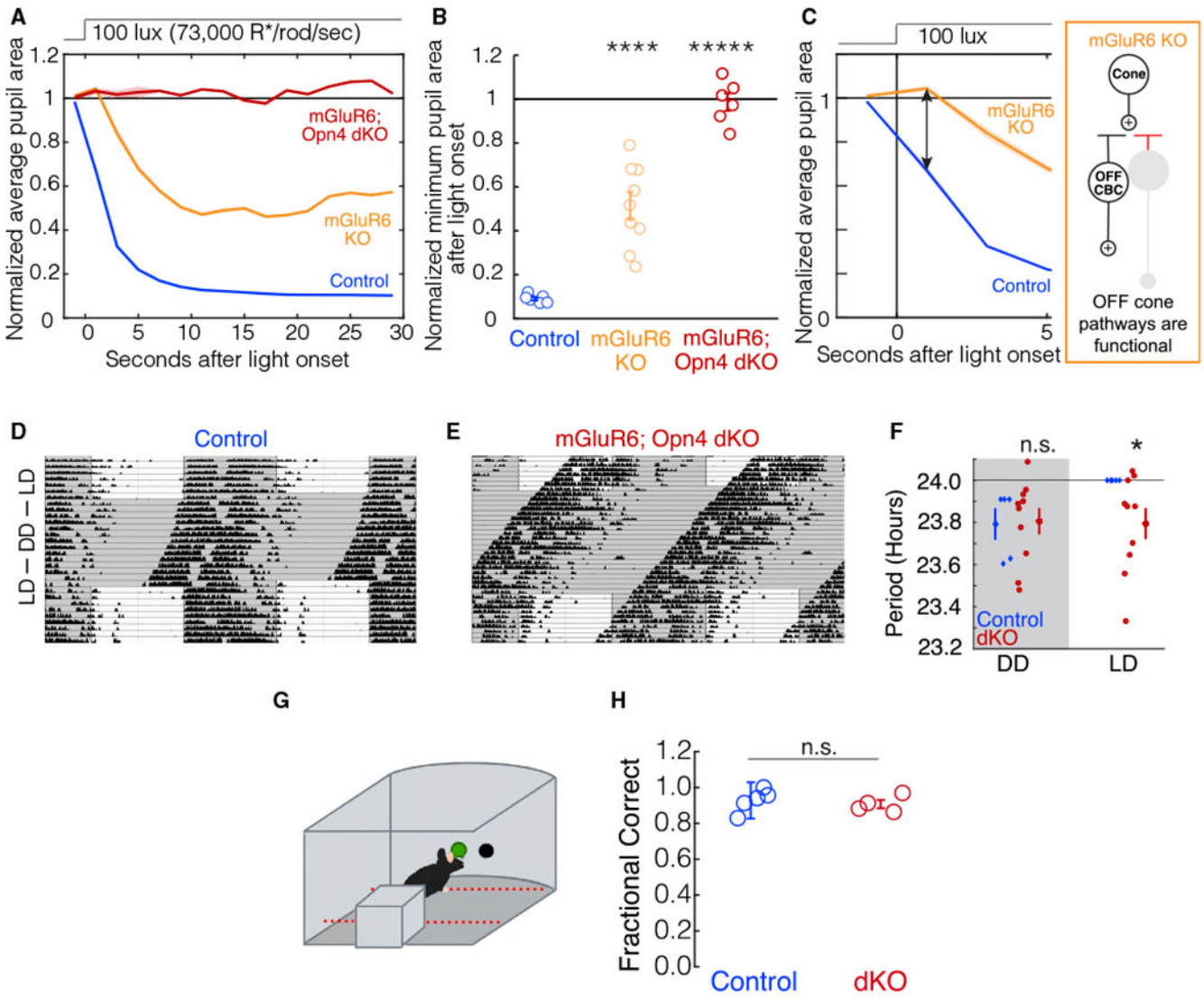

Figure 2. The OFF pathway cannot drive the PLR or circadian photoentrainment but does drive image-forming vision

(A) The average pupil constriction over time in response to 100-lux light (73,000 R*/rod/s) beginning at t = 0 s for control (blue, n = 6), mGluR6 KO (orange, n = 9), and mGluR6; Opn4 dKO (dark red, n = 6) mice. Shaded outlines represent SEM. All pupil sizes are normalized to the dark-adapted pupil size (before t = 0).

(B) The minimum normalized pupil area (maximal constriction) in response to 100-lux light from t = 0 to t = 30 s. Individuals are shown as circles. Error bars show SEM. Significance from the littermate control group is as follows: mGluR6 KO, p = 3E–5; mGluR6; Opn4 dKO, p = 3E–6 (ANOVA post hoc Dunnett's method).

(C) PLR delay seen in (A). mGluR6 KO mice (orange) have a pupil constriction deficit immediately after light onset (ANOVA post hoc Dunnett's method, p = 0.002). The mGluR6 mutation silences the cone ON pathway in these mice, as indicated by the circuit diagram.

(D) Littermate control mice confine their activity to the dark portions of the 12-h light – 12-h dark (12:12 LD) cycle (n = 5). Light and dark exposure is indicated by white and gray shading.

(E) mGluR6; Opn4 dKO mice do not confine their activity to the dark portions of the day and instead free run in 12:12 LD (n = 10).

(F) Quantification of period lengths from all animals (points indicate individual animals, error bars show SEM). Littermate control mice (blue) photoentrain to the light-dark cycle, as indicated by their period lengths equaling exactly 24 h. mGluR6; Opn4 dKO mice (red) free run in 12:12 LD, as indicated by their period lengths being similar in DD to LD. Littermate control and mGluR6; Opn4 dKO mice have comparable period lengths in DD (Student's t test, $p = 0.90$). In 12:12 LD, the mean period lengths of mGluR6; Opn4 dKO mice do not equal 24 h (Student's one-way t test, $p = 0.02$). See also Figures S1 and S2.

(G) Schematic depicting the visually guided behavioral task. Mice were trained in the two alternative forced choice paradigm to detect a light stimulus in one of two holes (STAR Methods). The testing chamber was kept dark except for the stimulus presented at photopic levels (28,000 R*/rod/s).

(H) Littermate control mice (blue, n = 5) correctly detect the light stimulus in the visually guided task (G) in ~90% of the trials. mGluR6; Opn4 dKO mice (dark red, n = 4) correctly detect the light stimulus comparable with control mice (Student's t test, $p = 0.59$). Error bars indicate SEM.

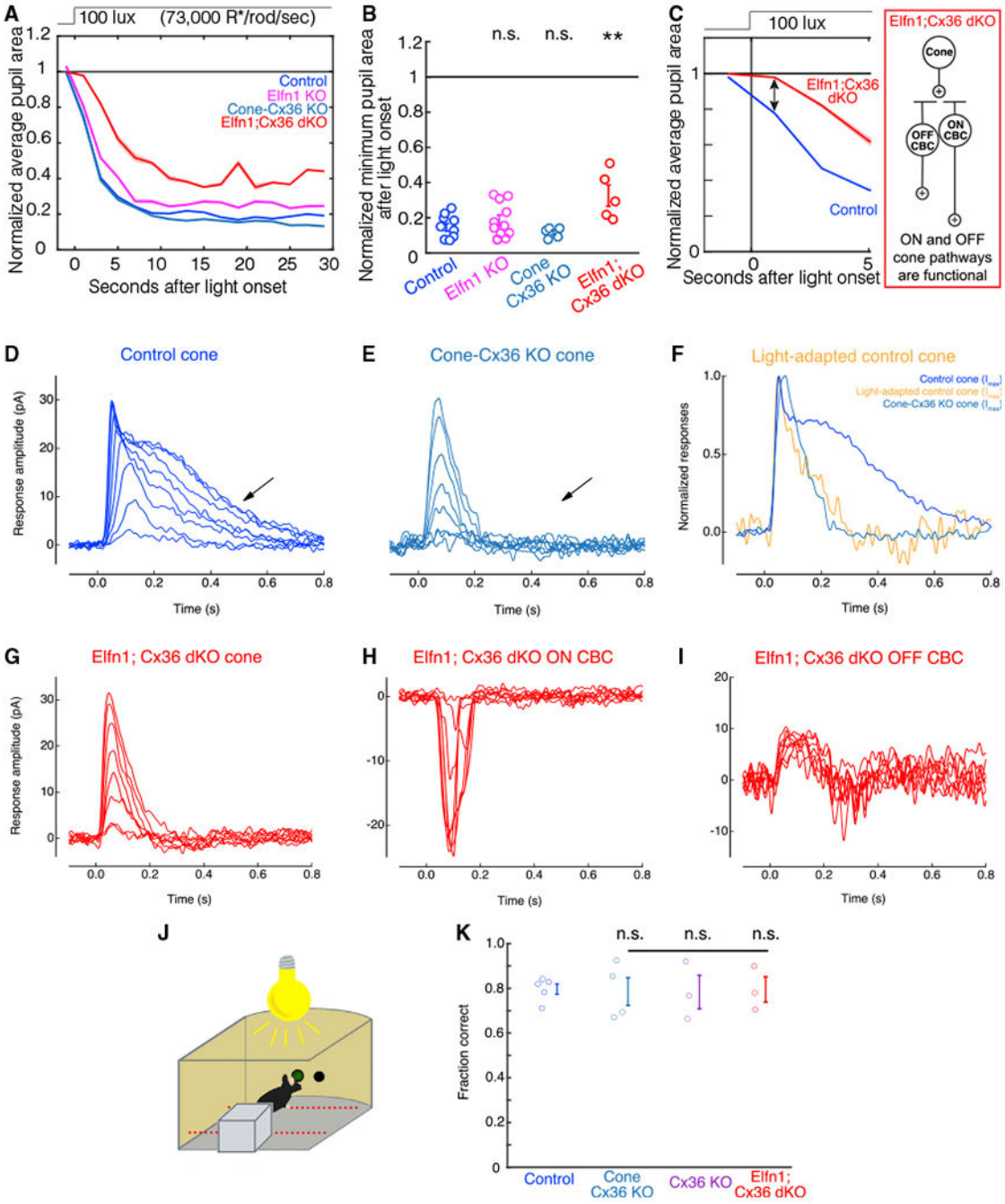

Figure 3. The primary and secondary rod pathways, not cone light responses, drive the photopic PLR

(A) The average pupil constriction over time in response to 100-lux light (73,000 R*/rod/s) beginning at t = 0 s (dashed line) for control (blue, n = 9), Elfn1 KO (magenta, n = 11), Cone-Cx36 KO (cyan, n = 5), and Elfn1; Cx36 dKO (red, n = 5) mice. Shaded outlines represent SEM. All pupil sizes are normalized to the dark-adapted pupil size (before t = 0). (B) The minimum pupil area (maximal constriction) in response to 100-lux light from t = 0 to t = 30 s. Individuals and SEM are shown. Significance from the control group is

as follows: Elfn1 KO, p = 0.58; Cone-Cx36 KO, p = 0.89; Elfn1; Cx36 dKO, p = 0.003 (ANOVA post hoc Dunnett's method).

(C) The PLR delay seen in (A). Elfn1; Cx36 dKO mice (red) have a pupil constriction deficit immediately after light onset compared with control mice (ANOVA post hoc Dunnett's method, p = 0.04). Cone pathways are functional in these mice, as indicated by the circuit diagram.

(D–F) Physiological recordings of cone photocurrents in retinal slices from littermate control and Cone-Cx36 KO mice. Recordings were made in whole-cell patch-clamp mode (V_m = −40 mV). 20-ms light flashes were given at time 0 s. Flash strength ranged from 3.1–203.4 R*/rod.

(D) In recordings from cones in control mice, a fast transient peak is followed by a slower sustained rod-dependent (arrow) response.

(E) In recordings from cones in Cone-Cx36 KO mice, the fast transient peak remains, but the slower sustained response is missing (arrow).

(F) A rod-suppressing background light (332 R*/rod/s) was applied to retinal slices in littermate control mice. In recordings from cones after light adaptation, the fast transient peak remains, but the slower sustained response is missing (yellow). Normalized responses from dark-adapted cones in Cone-Cx36 KO (cyan) and littermate control (blue) mice are shown for comparison.

(G–I) Physiological recordings of photopic light responses recorded in an Elfn1; Cx36 dKO retina slice. Recordings were the same as in (D), except that flash strength ranged from 31–2,034 R*/rod. Recordings are representative of data collected across several cells.

(G) Cone responses in Elfn1; Cx36 dKO mice are missing the rod-dependent sustained response.

(H) ON CBCs depolarize in response to a photopic light flash.

(I) OFF CBCs hyperpolarize in response to a photopic light flash.

(J) Schematic depicting the visually guided behavioral task with a rod-suppressing background light (3,500 R*/rod/s) illuminating the testing chamber. The light stimulus was presented at photopic levels (28,000 R*/rod/s).

(K) Quantification of the testing trials by control mice (blue, n = 5), Cone-Cx36 KO mice (cyan, n = 4), Cx36 KO mice (purple, n = 3), and Elfn1; Cx36 dKO mice (red, n = 3) under rod-suppressing background light. KO mice correctly detect the light stimulus with an accuracy comparable with controls under light-adapted conditions (ANOVA post hoc Dunnett's method, KO mice from control mice, all p > 0.99). Error bars indicate SEM.

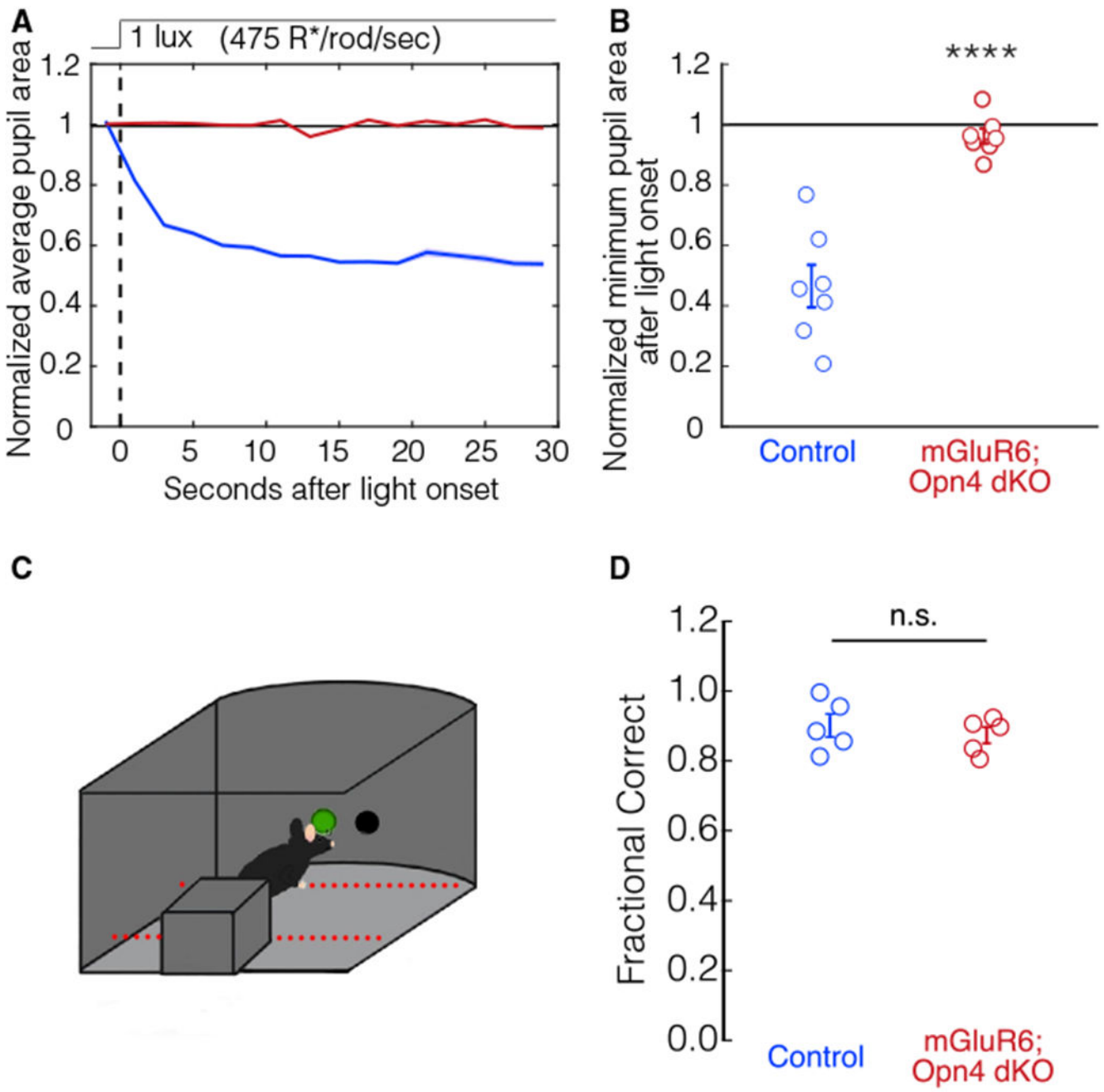

Figure 4. Rod OFF pathways drive scotopic image formation but do not drive the scotopic PLR

(A) The average pupil constriction over time in response to 1-lux light (475 R*/rod/s) beginning at t = 0 s (dashed line) for control (blue, n = 7) and mGluR6; Opn4 dKO (dark red, n = 7) mice. Shaded outlines represent SEM. All pupil sizes are normalized to the dark-adapted pupil size (before t = 0).

(B) The minimum pupil area (maximal constriction) in response to 1-lux light from t = 0 to t = 30 s. Individuals and SEM are shown. Pupil constriction in littermate control mice and mGluR6; Opn4 dKO mice is significantly different (Student's t test, p = 2E–5).

(C) Schematic depicting the visually guided behavioral task. Mice were dark adapted for 3 h before experiments, and the testing chamber was kept dark except for the scotopic light stimulus (200 R*/rod/s).

(D) Control mice (blue, n = 5) correctly detect the light stimulus in ~90% of the trials. mGluR6; Opn4 dKO mice (dark red, n = 5) correctly detect the light stimulus comparable with control mice under scotopic conditions (Student's t test, p = 0.51). Error bars indicate SEM.

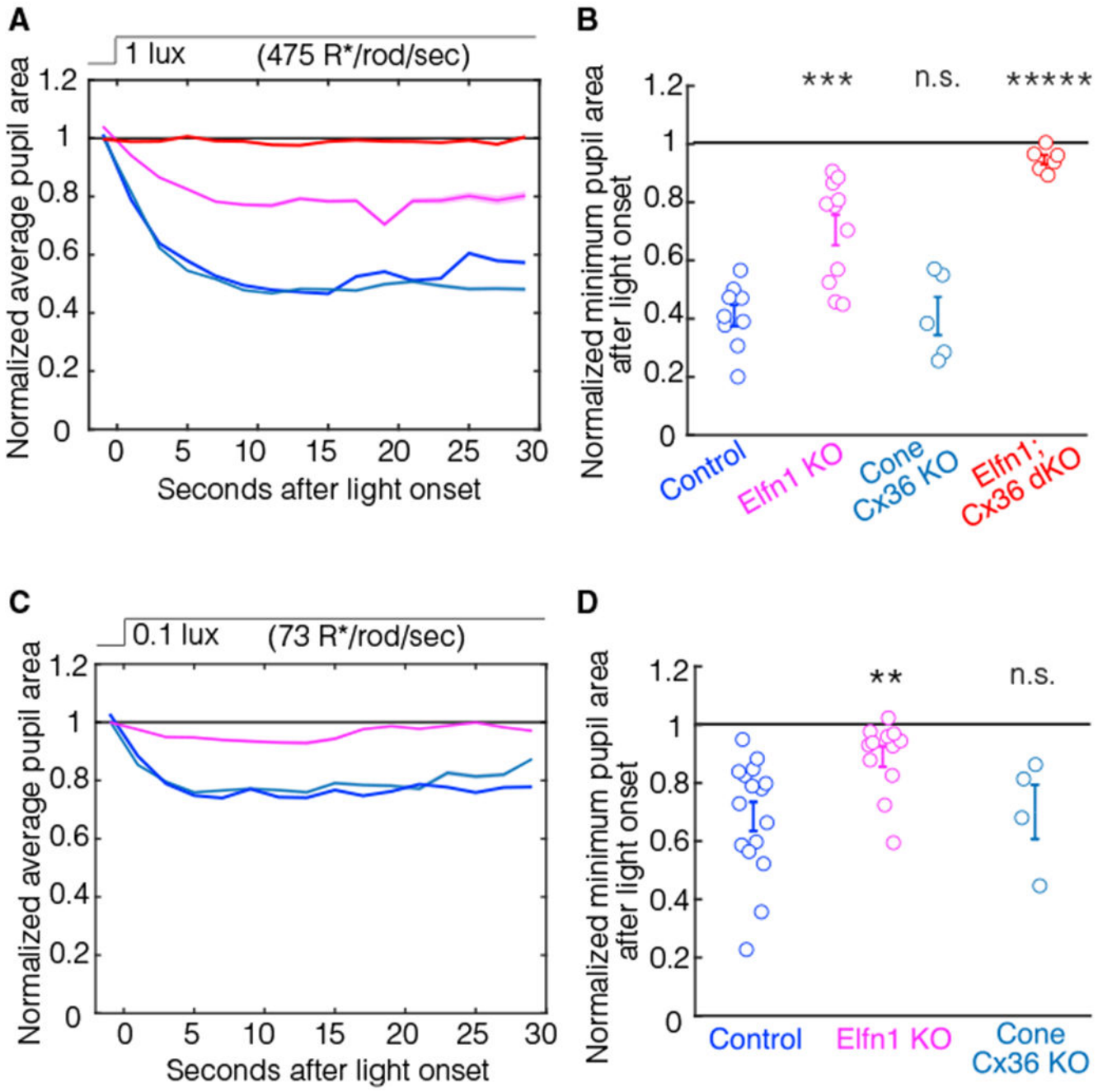

Figure 5. The primary rod pathway is required for the scotopic PLR

(A) The average pupil constriction in response to 1-lux light (475 R*/rod/s) beginning at t = 0 s for control (blue, n = 9), Elfn1 KO (magenta, n = 11), Cone-Cx36 KO (cyan, n = 5), and Elfn1; Cx36 dKO (red, n = 6) mice. Shaded outlines represent SEM. All pupil sizes are normalized to the dark-adapted pupil size (before t = 0).

(B) The minimum pupil area (maximal constriction) in response to 1-lux light from t = 0 to t = 30 s. Individuals and SEM are shown. Significance from the control group is as follows: Elfn1 KO, p = 1.3E–4; Cone-Cx36 KO, p = 1; Elfn1; Cx36 dKO, p = 2.7E–6 (ANOVA post hoc Dunnett's method).

(C) The same as (A) but a 0.1-lux light (73 R*/rod/sec) stimulus was used.
(D) The minimum pupil area (maximal constriction) in response to 0.1-lux light from t = 0 to t = 30 s. Individuals and SEM are shown. Significance from the control group (blue, n = 16) is as follows: Elfn1 KO (magenta, n = 12), p = 0.008; Cone-Cx36 KO (cyan, n = 4), p = 0.98 (ANOVA post hoc Dunnett's method).

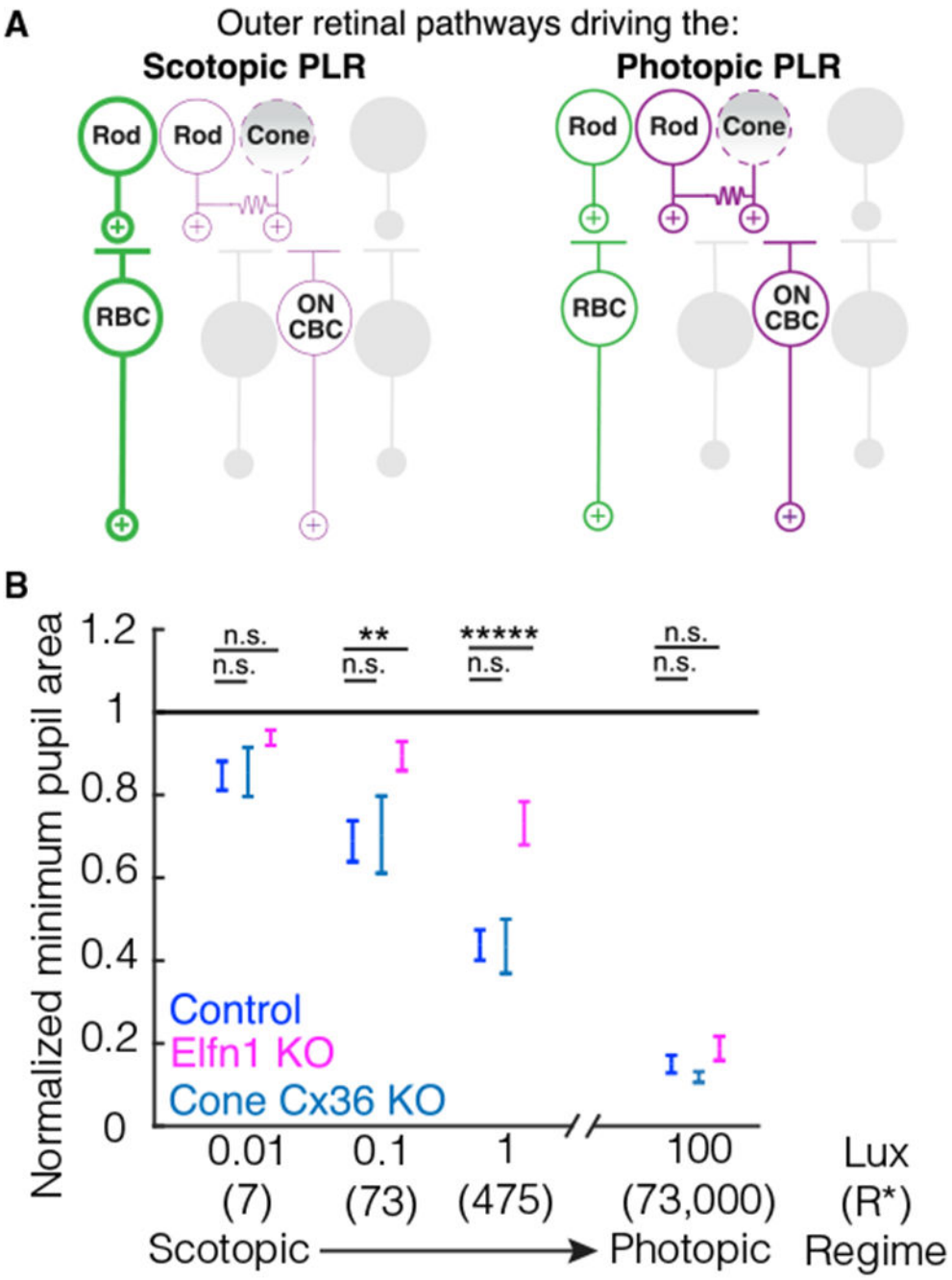

Figure 6. The outer retinal circuit pathways driving the PLR

(A) A schematic detailing the outer retinal circuit pathways that drive the photopic and scotopic PLR. Left: the primary rod pathway is the predominant circuit driving the scotopic PLR (bold green) and is required for normal pupil constriction. The secondary ON rod pathway (purple) cannot completely compensate for the primary rod pathway. The secondary OFF rod pathway and tertiary rod pathway cannot drive the scotopic PLR (gray). Cones cannot compensate for rods at scotopic light levels (indicated by a dashed outline and shaded gradient). Right: the primary rod pathway (green) and secondary ON rod pathway

(purple) can drive the normal photopic PLR. The secondary OFF rod pathway and tertiary pathway cannot drive the photopic PLR (gray). Cones cannot compensate for rods even when the secondary rod pathway drives the photopic PLR (indicated by a dashed outline and shaded gradient).

(B) Summary plot of control and mutant mouse pupil constriction across scotopic to photopic light levels. Data shown are summarized from Figures 3 and 5. Elfn1 KO mice, but not Cone-Cx36 KO mice, have deficits in their PLR under scotopic and mesopic light regimens. Error bars indicate SEM. Significance from the control group at each light level is as follows (ANOVA post hoc Dunnett's method): at 100-lux, Elfn1 KO $p = 0.58$, Cone-Cx36 KO $p = 0.89$; at 1-lux, Elfn1 KO $p = 1.3 \times 10^{-4}$ Cone-Cx36 KO $p = 1$; at 0.1-lux, Elfn1 KO $p = 0.008$, Cone-Cx36 KO $p = 0.98$; at 0.01-lux, Elfn1 KO $p = 0.33$, Cone-Cx36 KO $p = 0.99$.

Table 1.

Response properties of rods and BCs

	$I_{1/2}$ (R*/rod)				Imax (pA)			
	Rods	**RBCs**	**ON CBCs**	**OFF CBCs**	**Rods**	**RBCs**	**ON CBCs**	**OFF CBCs**
Wild type (WT)	18 ± 0.9 (8)	3.1 ± 0.4 (12)	7.2 ± 2.2 (8)	12.8 ± 2.2 (7)	27.1 ± 3.5 (8)	273.5 ± 37.1 (12)	18.3 ± 4.5 (9)	21.5 ± 4.6 (6)
mGluR6; OPN4 DKO	16.7 ± 1.2 (6)	− (4)	− (5)	8.8 ± 1.8 (4)	21.6 ± 4 (5)	− (4)	− (5)	14.7 ± 5 (4)
Elfn1 KO	14.5 ± 1.3 (6)	− (10)	6.4 ± 1.3 (10)	9.9 ± 0.6 (9)	27.4 ± 2.1 (7)	− (10)	13.2 ± 2.5 (10)	22 ± 3.2 (8)
Cone Cx36 KO	17 ± 0.7 (11)	3.6 ± 0.3 (7)	− (9)	14.2 ± 1.6 (7)	23.9 ± 1.6 (11)	355.3 ± 54.6 (7)	− (9)	12 ± 3.3 (7)
Elfn1; Cx36 DKO	19 ± 1.8 (5)	− (8)	− (9)	14.6 ± 2.3 (4)	24.2 ± 3 (5)	− (8)	− (9)	5.6 ± 1.1 (4)

Physiological properties of rods and BCs of the genotypes studied (n = number of mice). Values for single cells are given as mean ± SEM, total number of cells (n). The sensitivity ($I_{1/2}$) was derived from the best-fit Hill equation: $R + (R_{max} - R)/\left\{1 + \left[\frac{I_{1/2}}{I}\right]^n\right\}$. Max current (Imax) is the peak of the light-evoked current response. The sensitivity ($I_{1/2}$) between light-responsive cells in control and KO mice was not significantly different. Rod sensitivity was comparable across animals (ANOVA post hoc Tukey's method, all $p > 0.15$). RBC sensitivity was comparable between control and Cone-Cx36 KO mice (Student's t test, $p = 0.33$). ON CBC sensitivity was comparable between control and Elfn1 KO mice (Student's t test, $p = 0.77$). OFF CBC sensitivity was comparable across animals (ANOVA post hoc Tukey's method, all $p > 0.52$).

KEY RESOURCES TABLE

REAGENT or RESOURCE	SOURCE	IDENTIFIER
Chemicals, peptides, and recombinant proteins		
Ames Medium w/L-Glutamine	USBiological Life Sciences	Cat# A1372-25
Experimental models: Organisms/strains		
Opn4 knockout mice	Hattar Laboratory, (Ecker et al., 2010)	N/A
mGluR6 KO mice	The Jackson Laboratory	Stock number 016883
Elfn1 KO mice	Martemyanov Laboratory, (Cao et al., 2015)	N/A
Cx36 KO mice	a gift from the Dr. Jeffrey Diamond laboratory, (Deans et al., 2001)	N/A
Cone-Cx36 KO mice	Ribelayga Laboratory, (Jin et al., 2020)	N/A
Software and algorithms		
MATLAB	MathWorks	R2020b
Vital View	STARR Life Sciences	N/A
Igor Pro 8	WaveMetrics, Inc.	Version 8.03
Fiji	ImageJ	Version 2.1.0/1.53c
Other		
4K HD Camcorder	Sony	FDRAX3
IR Illuminators	ICAMI	96pcs
6500K A19/LED	Sunlite	10W E26
Foot Candle/Lux Light Meter	EXTECH	401025